The Role of Convective Moistening in the Madden-Julian Oscillation

Katherine Thayer-Calder*and David A. Randall

Colorado State University, Fort Collins, Colorado

Corresponding author address: Katherine Thayer-Calder, Colorado State University, Department of Atmospheric Science, Fort Collins, CO 80523. E-mail: katetc@atmos.colostate.edu

ABSTRACT

This study compares two models that differ primarily in their cloud parameterizations and produce extremely different simulations of the Madden-Julian Oscillation (MJO). The Community Atmosphere Model (CAM) version 3.0 from NCAR uses the Zhang-McFarlane scheme for deep convection and does not produce an MJO. The "superparameterized" version of the CAM (SP-CAM) replaces the cloud parameterizations with a two-dimensional cloud-resolving model (CRM) in each grid-column and produces an extremely vigorous MJO.

Our analysis shows that the CAM is unable to produce high-humidity regions in the mid- to lower-troposphere because of a lack of coupling between parameterized convection and environmental relative humidity. The SP-CAM produces an overly moist column, due in part to excessive near-surface winds and evaporation during strong convective events. In the real tropics and the SP-CAM, convection within a high-humidity environment produces intense latent heating, which excites the large-scale circulation that is the signature of the MJO. Our analyses suggest that a model must realistically represent convective processes that moisten the entire tropical troposphere in order to produce a simulation of the MJO.

1. Introduction

The Madden-Julian Oscillation (MJO), an intraseasonal oscillation of convection and winds in the tropical Indian and western Pacific oceans, is a very large, generally equatorial, eastward-propagating region of active convection, followed and/or preceded by an equally large eastward moving region of clearer skies and suppressed convection (Madden and Julian 1972, 1994). The MJO spans 50 to 100 degrees of longitude, or zonal wavenumbers 1 to 5, and its speed generally varies from 4 to 6 m s^{-1} (Zhang 2005). Observational studies of the MJO are reviewed by Madden and Julian (1994) and Zhang (2005). This massive convective disturbance has huge impacts on the weather and climate of our planet, but is not well understood. Currently no theory can adequately explain the processes and attributes of the MJO, and it is often poorly formed or completely missing in global climate simulations (Lin et al. 2006).

Slingo et al. (1996) provide an early view of the difficulties many global climate models (GCMs) have in representing the MJO. While most of the models discussed in their study produce large eastward-propagating convective disturbances, they generally move much faster than the observed MJO. A more recent study by Lin et al. (2006) reviews tropical precipitation in 14 GCMs from the Intergovernmental Panel on Climate Change (IPCC) Fourth Assessment Report (IPCC 2007), each coupled to an interactive ocean surface model. They show that the MJO-related precipitation variance is less than half of the observed tropical precipitation variance in 12 of the 14 models.

While many GCMs have trouble simulating the MJO, some modeling groups have been successful. Both Slingo et al. (1996) and Lin et al. (2006) point to the details of the models'

convective parameterizations as being the most important factors in the realism of their MJO simulations, and other studies support this conclusion. For example, Tokioka et al. (1988) are able to simulate an MJO, in a GCM that did not previously have such an oscillation, simply by imposing a minimum entrainment rate for penetrating convection. The minimum entrainment rate is proportional to the reciprocal of the mixed-layer depth. In this model, the most active intraseasonal oscillations form when the deep convective parameterization does not become active until the mixed layer is very thick and nearly saturated at its top.

Wang and Schlesinger (1999) examine three different convective parameterizations in their GCM, along with the effects of a minimum relative humidity requirement for the excitation of convection. Their results show that the choice of convective parameterization does affect the simulation of the MJO in the model, but the relative humidity criterion has a much larger impact. Increasing the required minimum relative humidity decreases the frequency of occurrence of deep convection in the models, leading to more time between strong convective events and higher tropical rainrate variability. The model that produces a very moist tropical atmosphere also produces a realistic intraseasonal oscillation in the region.

Raymond (2000) presents a simplified model for tropical convection, and applies it to intraseasonal oscillations in Raymond (2001). He obtains realistic results using the very simple assumption that rainfall is inversely proportional to the mean saturation deficit of the convective column. His idealized model produces strong, self-sustaining low-frequency oscillations similar to the observed MJO. Raymond (2001) proposes that the oscillations are maintained by a surface-flux feedback, in which convection leads to convergence near the surface, which produces stronger surface fluxes, which then reduce the column saturation

deficit. This leads to more convection, and the cycle continues.

Grabowski and Moncrieff (2004) also investigate the distribution of relative humidity in convective columns, and its effects on the MJO, in their GCM. Their study concludes that when convection occurs in a very moist environment, entrainment of moist air does not strongly dilute ascending parcels, and evaporation of precipitation is reduced. This strengthens the convective heating, which must be balanced by increased subsidence outside of the convective region, resulting in the formation of large-scale circulations. These large-scale circulations increase the depth of the moist layer in the convective region, and increase the subsidence of dry air outside of the region. This moisture-convective feedback maintains the circulation.

Very recently, the European Centre for Medium-range Weather Forecasts (ECMWF) adopted a new convective parameterization in their current operational forecast model (Bechtold et al. 2008). The Centre removed the previous controls of convection (moisture-convergence and large-scale lift), and replaced them with a simple parameterization that relates the convective mass flux of entraining plumes to their saturation deficit, so that the intensity of convection is controlled by the amount of vapor in the column. After this change, the tropical convective variability is much improved, and the amplitude of MJO events is more realistic. Also, midlatitude forecast skill improves slightly.

The various theories and hypotheses of the MJO involving a simple and direct relationship between precipitation and column moisture have been supported by observational studies such as that of Bretherton et al. (2004). Their study analyzes four years of gridded tropical rainfall and column vapor satellite measurements. They find a very strong non-linear but direct relationship between tropical rainfall and column-relative humidity [which is closely

and inversely related to the mean saturation deficit discussed by Raymond (2000)]. Although correlation does not imply causality, the link between heavy precipitation and increased column moisture is important. Bretherton et al. (2004) show that rainfall increases rapidly with column-relative humidity above 70%, which also supports the concept of a minimum or critical value of relative humidity for deep convection. These two observationally-based conclusions support theories that argue for the importance of a high-humidity environment for tropical deep convection.

Our study continues this analysis of relative humidity and its impact on tropical rainfall and the MJO. We begin with a comparison of two models which differ only in their convective parameterizations, and produce wildly different MJOs. The first is the NCAR Community Atmosphere Model (CAM) version 3.0, and the second is a superparameterized version of the CAM (SP-CAM) in which the convective parameterizations have been replaced with a two dimensional Cloud Resolving Model (CRM) in each GCM grid column (Khairoutdinov and Randall 2001). The CAM produces almost no recognizable MJO disturbances, and has very little power above the background spectrum for wave numbers and frequencies characteristic of the MJO. In contrast, the SP-CAM produces extremely vigorous MJOs, stronger even than most of the observed disturbances (Khairoutdinov et al. 2008; Benedict and Randall 2009). The differences in the results of the two models provide an opportunity to learn about which processes are important for the production and maintenance of a strong and healthy MJO, not just within a model but also in the real atmosphere.

2. Models

The analysis presented here uses four years of model output from the Community Atmosphere Model (CAM) v3.0, and four years of output from the superparameterized CAM (SP-CAM). Both models were run at Pacific Northwest National Laboratory (McFarlane et al. 2007), and both used the finite-volume dynamical core (Collins et al. 2004). NCAR has released a newer version of CAM (v3.5), but study of the 3.0 version is still relevant, as this model is the atmospheric component of the Community Climate System Model (CCSM3), used in the recent IPCC AR4 (Randall et al. 2007). Both the standard and superparameterized versions of CAM use the same AMIP-style boundary conditions (Gates 1992) for the period June 1998 through May 2002. Both versions have a grid spacing of 2° latitude, 2.5° longitude and 26 layers between 992 hPa and 3.5 hPa.

In the standard CAM, deep convection (Zhang and McFarlane 1995), shallow convection (Hack 1994) and stratiform clouds (Sundqvist 1988) are simulated using separate parameterizations. The SP-CAM replaces traditional convective parameterizations in each GCM grid column with a two dimensional CRM that solves the non-hydrostatic equations using the anelastic approximation. Details of the formulation of the CRM can be found in Khairoutdinov and Randall (2003), and more information on its implementation within the CAM can be found in Khairoutdinov and Randall (2001), Khairoutdinov et al. (2005), and Khairoutdinov et al. (2008). The 2D CRM in each grid column of the SP-CAM has 64 grid columns, each four kilometers wide, oriented in the east-west direction, and has periodic boundary conditions. There are 24 height-coordinate levels which roughly correspond to the lowest 24 of the 26 sigma-coordinate levels in the external GCM grid (the CAM grid). After each

GCM timestep, the CRM returns horizontal mean fields as tendencies or results due to cloud processes in each gridcell. The CRM is prevented from transferring momentum tendencies to the parent GCM due to the unrealistic two-dimensional dynamics. Radiative transfer for the SP-CAM is calculated within the CRM, and is performed interactively for each CRM grid column every 15 minutes.

The superparameterization has several important strengths relative to traditional parameterizations of convection. The explicit simulation of deep convection allows for better connections between small-scale processes such as microphysics and larger-scale processes such as cloud-scale dynamics. The explicit simulation of cloud geometry improves cloud-radiation interactions. Both the cloud-scale and mesoscale effects of downdrafts are included in the CRM. However, there are several drawbacks to superparameterization as well. The superparameterization slows down the GCM by roughly a factor of 200. While a four-kilometer grid spacing in the CRM is marginally acceptable for deep convection, small clouds and circulations are still unresolved. Finally, land-surface processes, including all surface fluxes (over both land and ocean) and orographic effects, are still calculated with the traditional parameterizations on the GCM grid in the SP-CAM. This means surface effects such as increased evaporation due to resolved convective processes (gust fronts or downdrafts) are not included in these simulations. A similar superparameterization has been implemented in the NASA Goddard Space Flight Center (GSFC) finite-volume GCM (fvGCM) (Tao et al. 2008).

Fig. 1 shows a histogram of the number of rainrate "observations" in the Indian Ocean and Western Pacific region (see Section 3b. for a description of the analysis domain) for the models as well as TRMM observations during the four year period. Rainrates are binned on

a logarithmically increasing scale. There are fewer days with the highest values of rainrate (both TRMM and SP-CAM drop to as few as 100), and the CAM does not have any days for the highest values. The CAM also has fewer rain-free days than the observations or the SP-CAM. This is consistent with the low tropical rainrate variability discussed in other studies (Khairoutdinov et al. 2005; Hack et al. 2006; Lin et al. 2006; Sun et al. 2006; DeMott et al. 2007), which generally conclude that the CAM convective parameterizations are triggered too often, resulting in persistant tropical drizzle rather than intense precipitation.

Fig. 1 shows that the SP-CAM has many more heavy rain days than the CAM, and, above about 1 mm hr^{-1}, more heavy rain days than observed in TRMM. This is evidence of the over-production of rain in the tropical regions of the SP-CAM, as described in Benedict and Randall (2009), DeMott et al. (2007), Luo and Stephens (2006), and others. Both models underestimate the number of days without rain in the deep tropics, and this results in the unrealistic secondary maxima of rainrates around 0.05 mm hr^{-1} (about 2 mm day^{-1}) in the SP-CAM and 0.5 mm hr^{-1} (about 12 mm day^{-1}) in the CAM.

Most of the heavy precipitation in the tropics of the CAM is produced by the Zhang-McFarlane scheme (as shown in Fig. 2). This parameterization describes the effects of the mass fluxes generated by a group of deep, penetrating convective updrafts and downdrafts, or cloud plumes. The scheme is triggered when conditional instability, corresponding to positive convective available potential energy (CAPE), develops in the column. As the updrafts in the ensemble of cloudy plumes lift warm moist air from the surface, and the downdrafts cool the lower levels, the net effect is to restore stability and reduce the CAPE (Zhang and McFarlane 1995). However, convective intensity may not be as connected to the amount of moisture in the column as recent observations suggest it should be (Bretherton

et al. 2004). While the dynamics of the scheme represent realistic processes at work in deep convection, many of the assumptions and parameters used are somewhat arbitrary. Within each grid column, all cloud tops and cloud updraft detrainment are forced to be above the mid-tropospheric minimum of saturation moist static energy (Collins et al. 2004). Constraining the updraft detrainment in this way limits the ability of the deep convection to moisten the lower troposphere. We will show how tropical convection is disrupted by these missing connections in the model.

3. Data and Methods

a. Observational Data

A variety of observational data are used in this study. The tropical precipitation data are from the TRMM gridded 3B42 product for dates June 1998 through May 2002. These give rainrates every three hours on a 0.25° by 0.25° grid over the tropics from calibrated IR merged with TRMM and other satellite data (Kummerow et al. 2000). The data are averaged to a 2.5° by 2.5° grid in order to match the model output.

Additional key observational resources for this study are the sounding and derived profile datasets from TOGA-COARE (Webster and Lukas 1992). During the Intensive Observation Period (IOP, November 1, 1992 through February 28, 1993), two convective episodes associated with the Madden-Julien Oscillation passed through the observational array (Yanai et al. 2000). We use merged profiler and rawinsonde observations of temperature and relative humidity from six sounding sites (Manus, Nauru, Kavieng, Kapinga, R/V Shiyan 3 and R/V

Kexue 1), tipping bucket rain gauge data from the six sites, and derived column profiles of heating rates based on budget analysis of soundings in the observational array (Ciesielski et al. 1997). Three-day-average rain and surface wind retrievals from the Special Sensor Microwave/Imager (SSM/I) Version-6 dataset, acquired from Remote Sensing Systems (Wentz and Spencer 1998), are also used.

The ERA-40 reanalysis product (Uppala et al. 2005) from the European Center for Medium Range Forecasting (ECMWF) is used throughout the study as a source for information on profiles of atmospheric variables that are difficult to observe. The ERA-40 datasets are on a 2.5° by 2.5° grid around the globe, and we use the same time periods used in the model data (June 1998 through May 2002). The vertical resolution of these data is coarser than that provided by the models (only 12 levels, from 1000 mb through 50 mb) so vertical profiles are plotted by interpolating onto the coarser ERA-40 levels, for ease of comparison.

Daily averaged low level winds from NCEP Reanalysis 2 data provided by NOAA/OAR/ESRL PSD, Boulder, Colorado, USA, (from their web site at http://www.cdc.noaa.gov/) are included as well (Kanamitsu et al. 2002).

b. Methods of Analysis

1) Domain and compositing method

We analyze several properties of the atmospheric column over the tropical warm pool as a function of rainrate in this study. These plots are created using the average daily rainrate in each 2.5° grid cell of the MJO Focus Region (MFR), which includes latitudes from 15°S

to 15°N and longitudes from 50°E to 180°E. Variables or profiles in each gridcell for all four years are binned and averaged together based on a logarithmically increasing rainrate scale. This method has also been used to analyze profiles of the equatorial Indian Ocean and Western Pacific, by Thayer-Calder (2008) and Kim et al. (2009). In this study, data from TOGA-COARE are binned (composited) and then smoothed with a three-bin running mean. ERA-40 data are generally binned using daily average TRMM rainrates from the same grid region, while NCEP data are binned using NCEP precipitation.

2) Identification of MJO events

MJO events are identified based on daily-averaged OLR between 15°S and 15°N (at all longitudes), using a filtering algorithm similar to that of Benedict and Randall (2007). First, the beginning and end of the timeseries are tapered using a simple normalization factor which reduces some spectral noise. Next, Fourier transforms are performed in space and then again in time, and power is calculated for all coefficients. Power outside of waveforms which fit the description of an MJO (zonal wavenumbers one to three and periods of 30 to 90 days) is set to zero, and the process is reversed. The result is data in the usual time-space domain, filtered to show only MJO-type waves. Finally, the filtered data are averaged across latitudes in the MFR into a longitude-time map of MJO strength.

To select MJO-active periods, the minimum values of averaged filtered OLR are selected from each day of longitude-time data. The location of minimum filtered OLR for each wet phase is used as the "day zero," corresponding to maximum wave intensity in composite wave passage plots. This day is determined by searching through negative anomalies of

filtered OLR greater than one standard deviation from the mean until a minimum is found, and then recording the longitude and day at that point (Fig. 3).

As mentioned earlier, the CAM does not produce a true MJO, but we have identified 13 "major" convective events in the region, and the nine found in the eastern hemisphere are used in our composites. There are 14 identified MJO events in the SP-CAM, and 12 of these are in the eastern hemisphere. For comparison, 16 MJO events are found in the ERA-40 OLR data for the same time period, 14 of which are in the eastern hemisphere.

3) Composite MJO passage

After the minimum filtered OLR has been selected for each of the MJO events, a composite plot in time can be made for that location. If we plot the evolution of a variable from 30 days before the minimum filtered OLR to 30 days after, we get a view of the atmosphere as one MJO event passes by. A composite wave passage plot has each day in the time series averaged with the corresponding day from all other MJO events. The result is an average portrait of the atmosphere as the MJO approaches the point of minimum filtered OLR and after it passes. Stephens et al. (2004), Benedict and Randall (2007), and many others create similar composite wave passage plots in their analyses.

4. Results

a. Efficiency of Tropical Convective Moistening

The composite profile of relative humidity as a function of rainrate, shown in Fig. 4, shows the effects of the disconnections between moisture and convective processes in the CAM, as described previously. This figure shows composite profiles of relative humidity for the MFR, as described in Section 3.b.1. In Fig. 4, the CAM (panel **a**) has a very dry layer below about 700 hPa and just above the boundary layer for all rainrates. The CAM is especially dry in this layer for heavy rainrates, when the deep convection parameterization is producing nearly all of the rain. The composite plot of relative humidity profiles from the SP-CAM (panel **b**) shows an overly moist column for middle intensity rainrates. The observations in panels **c** and **d** show that the atmosphere should only see a fully saturated column above the heaviest rainrates, and that the higher relative humidity in the mid-levels above middle intensity rainfall should not be completely saturated as it is in the SP-CAM. The ERA-40 and TOGA-COARE plots show that the very moist column for middle to higher rainrates in the SP-CAM is excessive, but more realistic than the CAM profile.

Fig. 5 shows the composite profiles of relative humidity for the selected events in the two models. As the MJO approaches the point of minimum filtered OLR in the SP-CAM, a thick layer of humid air forms up to above 600 hPa. As the heaviest convection passes at the point of minimum filtered OLR, the entire column experiences a high relative humidity. After the passage of the wave, the lower layer of moisture thins as drier air arrives near the surface and top of the layer. Similarly, both the ERA-40 and TOGA-COARE data show an increase in relative humidity through the boundary layer and the column before the passage

of the wave, and a rapid reduction in relative humidity afterwards.

The CAM, on the other hand, does not build up a thick layer of humid air. At the point of heaviest convection, near day zero, there is a hint of an increase in relative humidity between 700 and 500 mb, but, in general, the column is much drier, and the boundary layer does not thicken as much as is seen during the passage of an MJO in the SP-CAM or in the observations. In fact, the dry layer between 850 and 700 hPa seen in Fig. 4**a** is also discernible in Fig. 5**a**.

The composite profiles in Figs. 4 and 5 provide a glimpse into the important relationship between rainfall and tropospheric moisture. Both of these figures show that rainrates should increase in association with increasing amounts of moisture, but do not indicate if the precipitation is causing the increase in humidity or if an increase in humidity leads to higher rainrates, or both. Moisture budgets give insight into this puzzle. In Fig. 6, we plot the daily accumulation of precipitation, the total daily surface evaporation, and the daily change in total precipitable water (TPW, or total column water vapor) as functions of rainrate. The accumulated precipitation curves are all similar, as they are calculated directly through the summation of daily average rainrate (on the abscissa). The change in TPW plots also show a similar pattern. All three plots show drying for the highest values of rainrates, with the SP-CAM having the highest daily average drying rate. The SP-CAM and ERA-40 both show moistening for lower rainrates, but the CAM has mixed or no real change in TPW in this region.

The most obvious differences among the three plots in Fig. 6 are in the evaporation curves. While the two versions of the CAM increase evaporation with precipitation, ERA-40 data show a decrease in evaporation with increasing precipitation. Since all three models use

parameterizations for evaporation based on the bulk aerodynamic formula, it is surprising that they would differ so dramatically.

Fig. 7 explains the discrepancy. Surface wind speeds are a key input to most bulk evaporation formulations, and both the SP-CAM and CAM show an increase in surface wind speeds with increasing rainrates. The ERA-40, NCEP-2, TOGA-COARE and SSM/I near-surface windspeeds are included for comparison. Both ERA-40 and NCEP-2 wind speeds show little dependence on daily average rainrates in the region, with a possible decrease for high rainrates in ERA-40 and a slight increase in NCEP-2. TOGA-COARE winds also change very little with rainrate, but the 3-day averaged wind and rain retrievals from SSM/I show an increase in winds with increasing rainrates. It is difficult, from these data, to determine what a realistic relationship between surface winds and rainrates should look like.

Back and Bretherton (2005) give an in-depth analysis of the relationship between surface wind speeds and precipitation in the Pacific ITCZ. Their results indicate that the relationship is complicated, and very different for different regions, or at different relative humidities. In general, they see an increase in precipitation with increased wind speeds, especially during days when column relative humidity is high. In a composite of all rainrates and wind speeds over four years at 160E and 10N, they found no strong relationship between wind and precipitation.

b. Convection in a Moist Environment

The dry layer between 850 and 700 hPa in the CAM (Fig. 4) impacts the entire tropical troposphere of the model in various ways. Fig. 8 shows the composite static stability profiles

for increasing rainrates in the MFR. Both the CAM and SP-CAM have an area of increased static stability between 0 and 0.01 mm hr^{-1} and 850 and 700 hPa. This is likely due to a boundary forming between the drier air above, which is sinking and adiabatically warming, and lower level turbulently mixed air, which is moistened by water evaporated from the surface. Composite profiles of vertical velocity (not shown here) support this conclusion. A low-level stable layer is indicative of a trade inversion associated with light rainrates in the tropical warm pool of the CAM and SP-CAM. Neither the ERA-40 reanalysis nor the TOGA-COARE data have such a strong cap in the low-rain regimes.

Another interesting feature of the static stability composites is the region of increased stability above the freezing level for the highest values of precipitation in all four plots. This inversion is extremely strong in the CAM, with a layer of pronounced low stability below the melting level for high rainrates. Decreasing potential temperature below and increasing above indicates a cold layer near the melting level during heavy precipitation events in the CAM. While the melting of frozen precipitation does cool the air, this process is strongly exaggerated in the CAM, and the unrealistic cold spot is probably caused by the melting precipitation also evaporating into the drier air below (see Fig. 4). In the SP-CAM, ERA-40 and TOGA-COARE analysis, strong convection, and heavy rain, occur in a nearly saturated column. This prevents further evaporation of rainfall, and the exaggerated "cold spot" seen in the CAM.

Convection in a nearly saturated column implies an increased precipitation efficiency and substantially decreased atmospheric radiative cooling (ARC) in these heavy convective regimes. Bony and Emanuel (2005) showed that moisture and radiative feedbacks involving these processes can be important for determining the scale and phase speed of the MJO. In

order to determine the effects of moisture on sub-grid scale processes such as precipitation efficiency and the ARC, we examine convective moistening in the framework proposed by Yanai et. al. (1973). They define Q_1 and Q_2 as an apparent heat source and an apparent moisture sink due to sub-grid scale processes. Specifically, Q_2 is the sink of humidity due to condensation and turbulent vertical transport of water vapor.

As can be seen in Fig. 9, relationships between precipitation and moistening the troposphere are different between the two models. To begin with, the total magnitude of Q_2 during heavy rain events in the SP-CAM is much greater than in the traditional CAM. Where the SP-CAM sees a Q_2 drying rate maxima greater than 60 K day^{-1}, the CAM only sees values up to about 40 K day^{-1}. This is largely because the CAM does not produce rain events as intense as those of the SP-CAM, and for a given rainrate in the composite, the maximum values of drying in the column are similar. The SP-CAM also sees convective drying through a large portion of the column, where the drying in the traditional CAM is squeezed, or much lower in general, at and below about 700 hPa, due to the constraints of the deep convective detrainment in the Zhang-McFarlane scheme.

Finally, the moistening (negative Q_2) at lower rainrates is slightly more intense in the CAM than the SP-CAM. This maybe due to the highly stable layer associated with lower rainrates (see Fig. 8) suppressing turbulent and convective lifting of humidity into the mid troposphere. The dry, sinking, air above will also evaporate any cloud water that might make it through the trade inversion, and adds to the apparent moisture source. Also, in the SP-CAM, there is a tongue of moist air for middle intensity rainrates, which moves upwards from 850 to 500 hPa as rainrates increase. This feature is not as prominent in the CAM composite, indicating once more that the CAM's deep convective parameterization does not

effectively moisten the layers between 850 and 500 hPa.

Composite profiles of Q_2 binned by IFA averaged rainrates are presented in Fig. 9c. This panel looks quite a bit different from the models, as it only includes 120 profiles of data (daily average over the entire region). Because of this, there is are no profiles for local intense rain or local dry days. However, the general pattern is reproduced; low level moistening is associated with shallow convection and drying with deep convection. The strongest drying is above the 700 hPa level in the TOGA-COARE profiles, however, they are not as obviously pinched as in the CAM.

Plots of Q_2 for a composite MJO, shown in Fig. 10, reveal the importance of convective drying for the oscillation in the models and the real world. In the SP-CAM, as the MJO approaches, the heating and drying due to convection intensify, spread through the column, and then remain at a high value for several days during the period of average peak rainfall and minimum OLR. While the convection is heating and drying the upper levels so powerfully, a moistening trend appears below. After the peak rainfall, the moistening intensifies and spreads vertically through a deep layer of the mid-troposphere. Some qualitatively similar features can be seen in the TOGA-CORE plots. In this plot, Q_2 drying strengthens and moves into the upper levels of the troposphere as the peak rainrates approach. After the period of the most intense rainfall, a reduction in the intensity of the convective drying occurs along with a slight moistening signal in the very lowest levels, which is likely caused by evaporation during westerly wind-bursts. The CAM, however, does not follow this pattern. In general, drying occurs in the upper levels (between 500 and 200 hPa) for nearly the entire period. The drying does occasionally approach the intensity seen in the SP-CAM, but it does not persist for long. Throughout the entire period, there is generally a large addition

of vapor to middle levels (between 850 and 500 hPa) where the atmosphere is dry and cloud water or precipitation readily evaporate.

Our results show that the artificial constraint on detrainment in the deep convective parameterization of the traditional CAM leaves a signature throughout the tropical atmosphere. In this model, convection is incapable of producing a moist layer between 850 and 700 hPa, which results in a stronger trade inversion in light precipitation events, increased evaporation of rain from strong convective events, and a decrease in the depth and strength of convective heating and drying. The SP-CAM, on the other hand, is almost completely saturated through the column for most rainrates above 1 mm hr^{-1}. This results in weaker melting-level static stability, and very intense convective drying and latent heating during heavy precipitation events.

5. Discussion

a. Too Dry or Too Wet

We have shown that the tropical atmosphere of the CAM is much drier than the SP-CAM and observations. The total column water vapor is less for almost all rainrates (Fig. 11) and the dry region of the atmosphere above light rainrates and below 700 hPa at heavy rainrates is especially obvious (Fig. 4). The SP-CAM, however, is overly moist, with a nearly saturated column for all rainrates above about 1 mm hr^{-1}. Our investigation of the simulated moisture budgets shows that daily change in TPW in the CAM does not vary systematically with precipitation, except for drying at high rainrates (Fig. 6). The CAM also has very high

surface wind values for these high rainrates (Fig. 7), and these lead to strong evaporation and moisture convergence. This balances the removal of water via precipitation, resulting in little variability of TPW in the daily mean. The lack of moistening in the lower troposphere of the CAM could prevent the model from creating an environment that has negative moist static stability (Neelin and Held 1987). Raymond and Fuchs (2009) create a simple model of tropical oscillation and relate large-scale, intraseasonal oscillations in the tropical atmosphere to the presence of negative moist static stability. Their hypothesis that the MJO requires moisture mode instability is supported by the results shown here.

The SP-CAM produces a wider range of change in TPW with rainrate, with low rainrates adding moisture, and heavy rain events associated with intense convective drying (Fig. 6). Moistening during low rainrates indicates the presence of negative moist static stability, moisture mode instability, and the capability of the model to produce an MJO (Raymond and Fuchs 2009). The drying as a function of high rainrate might be even larger if the model did not also have very strong winds during heavy precipitation events, resulting in high evaporation and moisture convergence, which counter the convective drying (Fig. 7). In both the SP-CAM and the CAM, the surface winds may remain high during intense rain events because of the lack of convective momentum transport.

This increase in moisture fluxes with increasing precipitation could lead to a feedback in the models that would favor excessive rain events. As convection and precipitation attempt to dry out the nearly saturated column during heavy rain events, the strong low-level winds evaporate and advect more surface moisture, and counter-act the convective drying. The continuing low-level moisture convergence feeds the convection, causing it to strengthen rather than dry out and weaken. Such a convection-wind-evaporation feedback is described

by Luo and Stephens (2006). They conclude that unrealistically enhanced precipitation in the SP-CAM is associated with increased wind speeds and increased evaporation, especially in the western Pacific during Asian monsoon periods.

The actual relationship between surface wind and heavy tropical convection has not been well quantified. Back and Bretherton (2005) describe a complex relationship, in which wind generally increases with rainrates when the humidity is high. Several studies have pointed to the importance of low-level gustiness and surface vapor fluxes for the maintenance of tropical convection and waves (Shinoda et al. 1998; Araligidad and Maloney 2008; Sobel et al. 2008). However, observational studies of the MJO have also shown that the highest wind anomalies generally occur several days after the most intense precipitation (Zhang 2005; Benedict and Randall 2007). We were unable to determine what a realistic relationship should be, based on our analysis and further work is needed.

b. The Discharge-Recharge Cycle

Bladé and Hartmann (1993) describe a Discharge-Recharge Cycle (DRC) which regulates the time interval between MJO events. According to their theory, after 30 to 70 days of increasing moisture and instability with low- and mid-level clouds, the atmosphere over the tropical Indian Ocean reaches a tipping point and large-scale convection can be triggered. This deep, intense convection spawns a large-scale circulation that dries the air and shuts off convection. After this "discharge", the region returns to a drier regime, with deep convection suppressed by the sinking branch of the MJO circulation, and the recharge period begins again.

Our analysis shows a build-up of moisture through the column (Fig. 5) prior to heavy precipitation in the SP-CAM, while the CAM remains dry as heavy rain events approach. This prevents the DRC from working realistically in the CAM. As shown in Fig. 11, the SP-CAM and observations show a correlated increase in precipitation and total precipitable water (TPW) during the DRC cycle, with rainrates and TPW increasing together during the recharge period and decreasing together during the discharge period. Due to the unrealistic relationships between moistening and precipitation in the CAM, the sequence is quite different. In the recharge period of the CAM, rainrates first increase with little increase in TPW, then TPW increases after rainrates have already peaked and started to decrease. This prevents the CAM from priming the environment for deep convection during the recharge period, and prevents a transition to a powerful discharge period. The DRC cannot operate, and no MJO appears.

Results from observed composited events (ERA-40 and TOGA-COARE) also show a strong correlation between moisture in the column and precipitation during an MJO (Fig. 11). The "loop" for the TOGA-COARE cycle is based on composites of one event at six location in the tropical western pacific. During this event, the direction of the loop is opposite of the other composites, indicating that the column was more moist before the passage of the wave than after. Whether this is the correct, or most realistic relationship is not known at this point. This directional difference could be due to the single MJO event or the location of the observational sites.

We can see why the interactions of convection and water vapor are so critical to the MJO by looking at Q_2. Figs. 5 and 11 show that the discharge period is a time of intense precipitation in a nearly saturated column. When convection occurs under these conditions,

it is possible evaporation of precipitation is inhibited, downdrafts are weaker, and convection is less effective in reducing instability. With weaker stabilization, convection intensifies. The end result is stronger condensation, heavier rainrates, and more intense upper-level latent heating.

As predicted by the models of Gill (1980) and Matsuno (1966), this rapidly intensifying heat source excites a large-scale circulation, which transports energy out of the region at upper levels and advects in cooler, drier air from the subtropics at lower levels. Fig. 12 shows the large-scale wind and relative humidity patterns simulated by the CAM and SP-CAM in one convective event in each model. In the SP-CAM, strong southwesterly winds at the intersection of two Rossby gyres advect drier air in below the intense convection (the map is centered at the location of minimum filtered OLR). The CAM, however, does not produce this surrounding large-scale structure. It does not produce the intense heating required to spawn vigorous large-scale wave and circulation patterns.

6. Concluding Discussion

The mystery of the missing MJO in many GCMs has been a source of much debate, discussion, and experimentation. This study analyzes output from two model simulations which differ only in their convective parameterizations, but produce very different MJO signals. The CAM, with the Zhang and McFarlane (1995) deep convective parameterization, does not simulate an MJO. The SP-CAM, with an embedded 2-D CRM replacing traditional convective parameterizations, creates an overly powerful oscillation.

We begin with a discussion of the deep convective parameterization in the CAM, and

point out two important missing connections between the convective mass transport and the water vapor profile. First, the deep convective scheme is triggered by CAPE, and may not be sensitive enough to the amount of moisture in the column. This allows strong convection in a dry column, which is shown to be unrealistic. Second, moisture must be detrained above the minimum of tropospheric saturation moist static energy, which prevents convection from moistening mid- and lower-tropospheric air. The SP-CAM more realistically couples convection and environmental humidity.

Our study shows that the CAM has a much lower rainrate variability than the SP-CAM (Fig. 1), and that relatively intense rain events occur in a drier environment in the CAM than in the SP-CAM (Fig. 4). These two results illustrate the two moisture-convection disconnects in the CAM, as described above. A model in which convection is not sufficiently sensitive to the humidity will likely produce weak convection too often. Also, a model that requires all deep convective detrainment to occur above the minimum saturation moist static energy will be unable to adequately moisten the entire column, leaving a dry layer in the lower troposphere, as seen in the CAM.

These same figures show that the SP-CAM has too many days with high rainrates, and an overly-moist column on those days. We show evidence that the nearly saturated tropical atmosphere in the SP-CAM is formed by an over-active convection-wind-evaporation feedback. When heavy precipitation occurs in the SP-CAM, the surface wind tends to be strong, increasing evaporation and further strengthening the convection.

Our study, and others (Tokioka et al. 1988; Wang and Schlesinger 1999; Raymond 2001; Grabowski and Moncrieff 2004), provide evidence that, in order to simulate a realistic MJO, a model must be able to create high humidity through a large portion of a tropical atmospheric

column. There are at least two possible interpretations of this need for high humidity, which do not contradict each other and can both be right.

The first is that high humidity makes it easier for convective clouds to penetrate through the depth of the troposphere without dilution by entrainment of dry air. Tokioka et al. (1988) show that an imposed minimum fractional entrainment rate inversely proportional to the boundary-layer depth permits an MJO to develop in a model that does not produce an MJO when non-entraining clouds are permitted. The minimum entrainment rate ensures that even the deepest convective clouds are sensitive to the environmental humidity above the boundary layer, so that deep clouds can form only when the sounding is sufficiently humid. Grabowski and Moncrieff (2004) support this idea as well.

A second interpretation of the need for high humidity, which can be traced to a suggestion by Emanuel (1989), is that high humidity inhibits downdrafts that would otherwise stabilize the sounding by reducing the moist static energy of the boundary layer air. Raymond (1995) argues that quasiequilibrium over the tropical oceans is primarily a balance between convective destabilization by surface evaporation (and radiative cooling), and convective stabilization through drying of the boundary-layer air by downdrafts. This boundary-layer quasiequilibrium is disrupted when the column humidity becomes high enough to inhibit the formation of downdrafts. As Emanuel (1989) wrote in the context of tropical cyclogenesis, "When the lower troposphere is sufficiently moist, the downdrafts can no longer counter the moistening of the subcloud layer by surface fluxes, deep HPE [high precipitation efficiency] convection breaks out in the core, and intensification begins." The same idea can apply to formation and intensification of the MJO. In fact, Bony and Emanuel (2005) argue for the relevance of this mechanism in their theory of the MJO.

Our analysis also shows that in order to have a realistic DRC, heavy precipitation should occur in a deeply moistened environment. The SP-CAM, ERA-40 and TOGA-COARE have a high relative humidity and large TPW for high rainrates, and all show increasing TPW with low rainrates. The CAM, however, is unable to deepen the moist layer though the entire column, unable to grow convection from low, to mid, to high levels, unable to produce a convective heat source that is sufficiently intense to spawn the large-scale circulation of the MJO. This results in a mal-formed DRC, in which convection is disconnected from environmental relative humidity, so that rainrates and TWP do not increase and decrease together coherently over the course of a Discharge-Recharge cycle.

In this study, we have gained some insight into the limits of the classic convective parameterization in the CAM, which does not produce an MJO. We find that the DRC is a useful way of interpreting the cycle of the MJO in both the models and the observations, but it does not explain all aspects of the MJO. The SP-CAM and other GCMs are powerful but imperfect tools for understanding tropical oscillations. Future work should include improving the feedbacks between convection and the large-scale circulation in the SP-CAM, and improving conventional convection parameterizations as well. Finally, we need to continue using these tools to improve our understanding the complex nature of tropical convection, and hopefully we will find a theory that adequately explains all of the processes and features of the MJO and other tropical disturbances.

Acknowledgments.

Special thanks to Roger Marchand, Steven Ghan, Nathaniel Beagley, and Tom Ackerman

for their help in procuring the data and answering many questions. Thanks to the CMMAP team for discussion and support. This work was funded by a National Science Foundation (NSF) grant ATM-0415184. This research was partially supported by the Office of Science (BER), U.S. Department of Energy, Cooperative Agreement No. DE-FC02-01ER63163. This work was also supported in part by the National Science and Technology Center for Multi-Scale Modeling of Atmospheric Processes (CMMAP), managed by Colorado State University under Cooperative Agreement ATM-0425247.

REFERENCES

Araligidad, N. M. and E. D. Maloney, 2008: Wind-driven latent heat flux and the intraseasonal oscillation. *Geophys. Res. Lett.*, **35**, L04 815, doi:10.1029/2007GL032746.

Back, L. E. and C. Bretherton, 2005: The Relationship between Wind Speed and Precipitation in the Pacific ITCZ. *J. Climate*, **18**, 4317–4328.

Bechtold, P., M. Kohler, T. Jung, F. Doblas-Reyes, M. Leutbecher, M. J. Rodwell, F. Vittart, and G. Balsamo, 2008: Advances in simulating atmospheric variability with the ECMWF model: From synoptic to decadal time-scales. *Quart. J. Roy. Meteor. Soc.*, **134**, 1337–1351, doi:10.1002/qj.289.

Benedict, J. J. and D. A. Randall, 2007: Observed Characteristics of the MJO Relative to Maximum Rainfall. *J. Atmos. Sci.*, **50**, 2922–2939.

Benedict, J. J. and D. A. Randall, 2009: Madden-Julian Oscillation Structure in the Superparameterized CAM. *Submitted to J. Atmos. Sci.*

Bladé, I. and D. L. Hartmann, 1993: Tropical intraseasonal oscillations in a simple nonlinear model. *J. Atmos. Sci.*, **50**, 2922–2939.

Bony, S. and K. Emanuel, 2005: On the role of moist processes in tropical intraseasonal variability: Cloud-radiation and moisture-convection feedbacks. *J. Atmos. Sci.*, **62**, 2770–2789.

Bretherton, C., M. E. Peters, and L. E. Back, 2004: Relationships between Water Vapor Path and Precipitation over the Tropical Oceans. *J. Climate*, **17**, 1517–1528.

Ciesielski, P. E., L. M. Hartten, and R. H. Johnson, 1997: Impacts of merging profiler and rawinsonde winds on TOGA COARE analyses. *J. of Atmos. Oceanic Tech.*, **14**, 1264–1279.

Collins, W. D., et al., 2004: Description of the NCAR Community Atmosphere Model (CAM 3.0). *NCAR Technical Note*.

DeMott, C. A., D. A. Randall, and M. F. Khairoutdinov, 2007: Convective precipitation variability as a tool for general circulation model analysis. *J. Climate*, **20**, 91–112, doi: 10.1175/JCLI3991.1.

Emanuel, K., 1989: The Finite-Amplitude Nature of Tropical Cyclogenesis. *J. Atmos. Sci.*, **46**, 3431–3456.

Gates, W. L., 1992: AMIP: The Atmospheric Model Intercomparison Project. *Bull. Am. Meteorol. Soc.*, **73**, 1962–1970.

Gill, A. E., 1980: Some simple solutions for heat-induced tropical circulation. *Quart. J. Roy. Meteor. Soc.*, **106**, 447–462.

Grabowski, W. W. and M. W. Moncrieff, 2004: Moisture-convection feedback in the tropics. *Quart. J. Roy. Meteor. Soc.*, **130**, 3081–3104, doi:10.1256/qj.03.135.

Hack, J. J., 1994: Parameterization of moist convection in the National Center for Atmospheric Research Community Climate Model (CCM2). *J. Geophys. Res..*, **99**, 5551–5568.

Hack, J. J., J. M. Caron, S. G. Yeager, K. W. Oleson, M. K. Holland, J. E. Truesdale, and P. J. Rasch, 2006: Simulation of the global hydrological cycle in the CCSM Commuity Atmosphere Model Version 3 (CAM3): Mean features. *J. Climate*, **19**, 2199–2221.

IPCC, 2007: *Climate Change 2007: The Physical Science Pasis. Contribution of Working Group I to the Fourth Assessment Report of the Intergovernmental Panel on Climate Change*. Cambridge University Press, Cambridge, United Kingdom and New York, NY, USA.

Kanamitsu, M., W. Ebisuzaki, J. Woollen, S.-K. Yang, J. J. Hnilo, M. Fiorino, and G. L. Potter, 2002: Ncep-deo amip-ii reanalysis (r-2). *Bull. Am. Meteorol. Soc.*, 1631–1643.

Khairoutdinov, M. F., C. DeMott, and D. A. Randall, 2008: Evaluation of the simulated interannual and subseasonal variability in an amip-style simulation using the csu multiscale modeling framework. *J. Climate*, **21**, doi:10.1175/2007JCLI1630.1.

Khairoutdinov, M. F. and D. A. Randall, 2001: A cloud resolving model as a cloud parameterization in the NCAR Community Climate System Model: Preliminary results. *Geophys. Res. Lett.*, **28**, 3617–3620.

Khairoutdinov, M. F. and D. A. Randall, 2003: Cloud resolving modeling of the ARM Summer 1997 IOP: Model formulation, results, uncertainties, and sensitivities. *J. Atmos. Sci.*, **60**, 607–625.

Khairoutdinov, M. F., D. A. Randall, and C. DeMott, 2005: Simulations of the atmospheric general circulation using a cloud-resolving model as a super-parameterization of physical processes. *J. Atmos. Sci.*, **62**, 2136–2154.

Kim, D., et al., 2009: Application of MJO Simulation Diagnostics to Climate Models. *Submitted to J. Climate.*

Kummerow, C., et al., 2000: The status of the tropical rainfall measuring mission (TRMM) after two years in orbit. *J. Appl. Meteor.*, **39**, 1965–1982.

Lin, J., et al., 2006: Tropical intraseasonal variability in 14 IPCC AR4 Climate Models. Part I: Convective signals. *J. Climate*, **19**, 2665–2690.

Luo, Z. and G. L. Stephens, 2006: An enhanced convection-wind-evaporation feedback in a superparameterization GCM (SP-GCM) depiction of the Asian sumer monsoon. *Goe. Res. Let.*, **33**, L06 707, doi:10.1029/2005GL025060.

Madden, R. A. and P. R. Julian, 1972: Description of global-scale circulation cells in the tropics with a 40-50 day period. *J. Atmos. Sci.*, **29**, 1109–1123.

Madden, R. A. and P. R. Julian, 1994: Observations of the 40-50- day tropical oscillation - a review. *Mon. Wea. Rev.*, **122**, 814–837.

Matsuno, T., 1966: Numerical integration of the primitive equations by a simulated backward differencing method. *J. Meteor. Soc. Japan*, **44**, 25–43.

McFarlane, S. A., J. Mather, and T. P. Ackerman, 2007: Analysis of tropical radiative heating profiles: A comparison of models and observations. *J. Geophys. Res.*, **112**, D14 218, doi: 10..1029/2006JD008290.

Neelin, J. D. and I. M. Held, 1987: Modeling tropical convergence based on the moist static energy budget. *Mon. Wea. Rev.*, **115**, 3–12.

Randall, D. A., et al., 2007: *Climate Models and Their Evaluation. In: Climate Change 2007: The Physical Science Pasis. Contribution of Working Group I to the Fourth Assessment Report of the Intergovernmental Panel on Climate Change*. Cambridge University Press, Cambridge, United Kingdom and New York, NY, USA, United Kingdom and New York, NY, USA.

Raymond, D. J., 1995: Regulation of Moist Convection over the West Pacific Warm Pool. *J. Atmos. Sci.*, **52**, 3945–3959.

Raymond, D. J., 2000: Thermodynamic control of tropical rainfall. *Quart. J. Roy. Meteor. Soc.*, **126**, 889–898.

Raymond, D. J., 2001: A new model of the Madden-Julian oscillation. *J. Atmos. Sci.*, **58**, 2807–2819.

Raymond, D. J. and Z. Fuchs, 2009: Moisture modes and the madden-julian oscillation. *J. Climate*, In Press.

Shinoda, T., H. H. Hendon, and J. Glick, 1998: Intraseasonal Variability of Surface Fluxes and Sea Surface Temperature in the Tropical Western Pacific and Indian Oceans. *J. Climate*, **11**, 1685–1702.

Slingo, J. M., et al., 1996: Intraseasonal oscillations in 15 atmospheric general circulation models: Results from an AMIP diagnostic subproject. *Climate Dyn.*, **25**, 117–140.

Sobel, A. H., E. D. Maloney, G. Bellon, and D. M. Frierson, 2008: The role of surface heat fluxes in tropical intraseasonal oscillations. *Nature Geoscience*, doi:10.1038/ngeo312.

Sun, Y., S. Solomon, A. Dai, and R. W. Portmann, 2006: How often does it rain? *J. Climate*, **19**, 916–934.

Sundqvist, H., 1988: *Parameterization of condensation and associated clouds in models for weather pediction and general circulation simulation.* Kluwer Academic, 433-461 pp.

Tao, W.-K., et al., 2008: A Multi-scale Modeling System: Developments, Applications and Critical Issues. *Bull. Am. Meteorol. Soc.*, In Press.

Thayer-Calder, K., 2008: The role of moisture in the MJO: A comparison of tropical convection processes in the CAM and Super-Parameterized CAM. MS Thesis, Atmospheric Science, Colorado State University, Fort Collins, Colorado.

Tokioka, T., K. Yamazaki, A. Kitoh, and T. Ose, 1988: The equatorial 30-60 day oscillation and the Arakawa-Schubert penetrative cumulus parameterization. *J. Meteor. Soc. Japan*, **66 (6)**, 883–901.

Uppala, S. M., et al., 2005: The ERA-40 re-analysis. *Quart. J. Roy. Meteor. Soc.*, **131**, 2961–3012, doi:10.1256/qj.04.176.

Wang, W. and M. E. Schlesinger, 1999: The dependence on convection parameterization of the tropical intraseasonal oscillation simulated by the UIUC 11-layer atmospheric GCM. *J. Climate*, **12**, 1423–1457.

Webster, P. J. and R. Lukas, 1992: TOGA COARE: The Couple Ocean-Atmosphere Response Experiment. *Bull. Am. Meteorol. Soc.*, **73**, 1377–1416.

Wentz, F. J. and R. W. Spencer, 1998: SSM/I rain retrievals within a unified all-weather ocean algorithm. *J. Atmos. Sci.*, **55**, 1613–1627.

Yanai, M., S. Ebensen, and J.-H. Chu, 2000: The Madden-Julian Oscillation Observed during the TOGA COARE IOP: Global View. *J. Atmos. Sci.*, **57**, 2374–2396.

Zhang, C., 2005: Madden - Julian Oscillation. *Rev. Geophys.*, **43**, RG2003, doi:10.1029/2004RG000158.

Zhang, G. J. and N. A. McFarlane, 1995: Sensitivity of climate simulations to the parameterization of cumulus convection in the CCC-GCM. *Atmos.-Ocean*, **3**, 407–446.

List of Figures

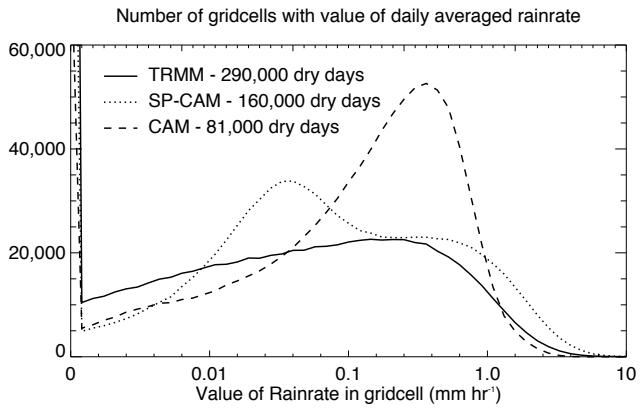

FIG. 1. Histogram of data points in each rainrate bin from TRMM, SP-CAM and CAM in the MFR between June 1998 and June 2002.

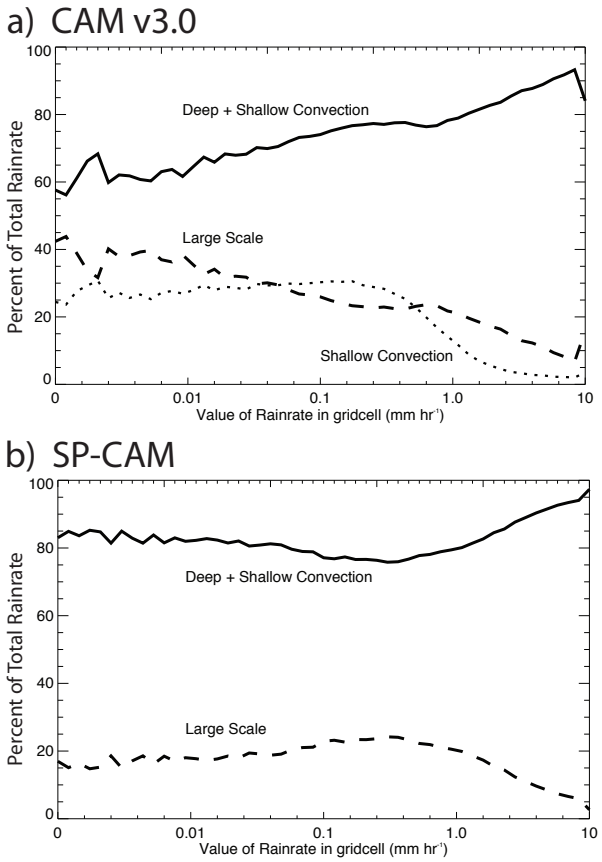

FIG. 2. The percentage of precipitation which originates from each parameterization per daily average rainrate for the two models. All precipitation in the SP-CAM originates in the embedded CRM, but rainrates above 10 mm hr^{-1} in a CRM column are categorized as convective and rainrates below this amount are categorized as Large-Scale.

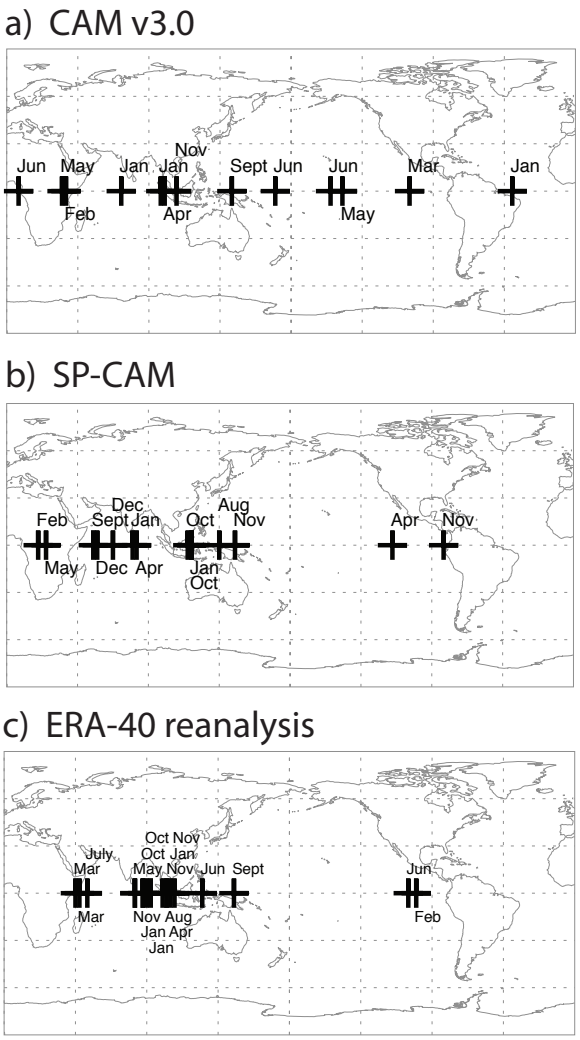

FIG. 3. Maps of the longitudinal location of each point of minimum filtered OLR, along with the month in which the labeled convective event occurred. Only events in the eastern hemisphere were used in this analysis.

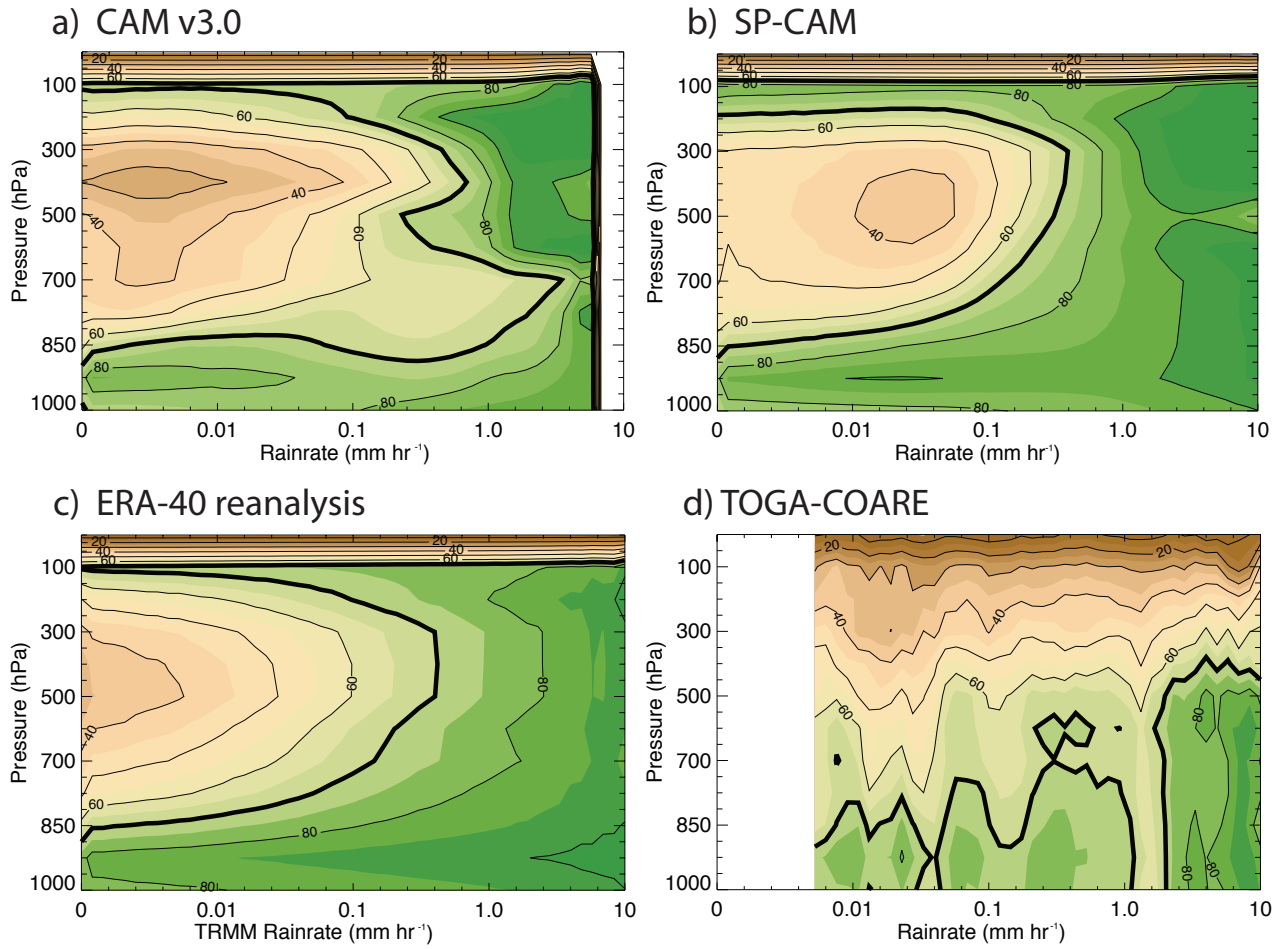

FIG. 4. Composite profiles of relative humidity binned by daily average rainrate in the MFR. Contour lines are in 10% increments. The 70% contour is darkened for clarity.

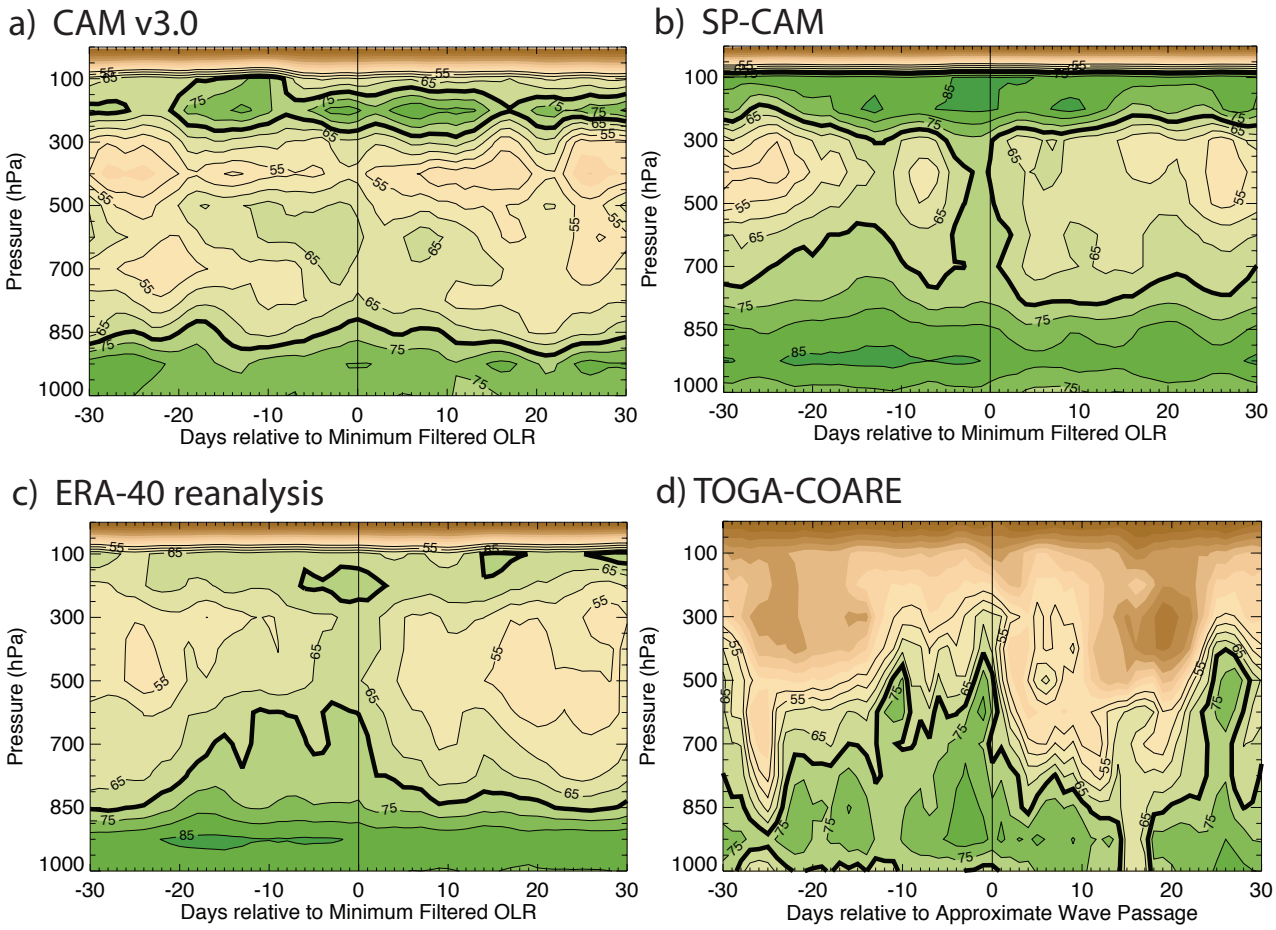

FIG. 5. Composite profiles of relative humidity with the passage of an MJO or strong convective event. Contour lines are in 5% increments and values below 50% relative humidity are not contoured. The 70% contour is darkened for clarity.

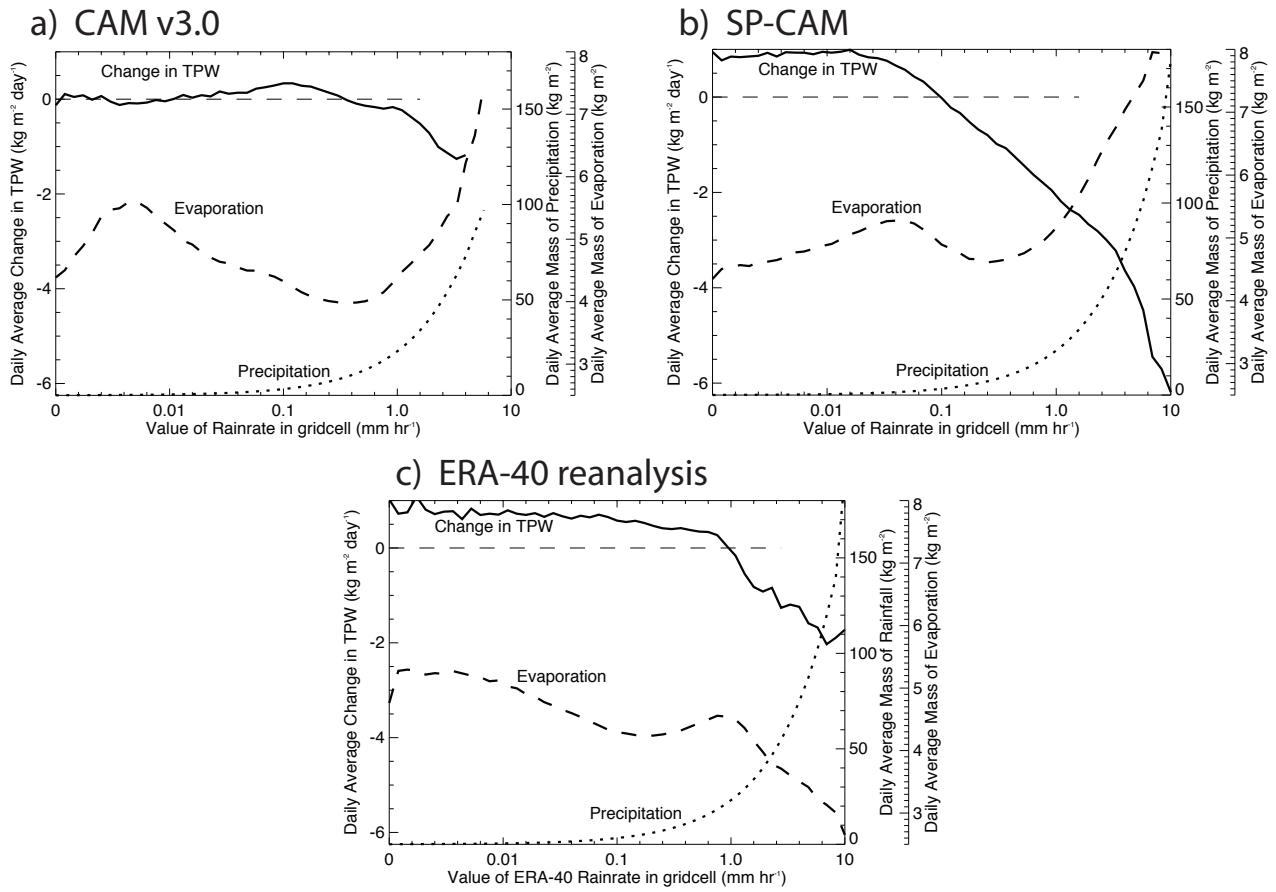

FIG. 6. Composite profiles of daily mass of precipitation, daily mass of evaporation, and daily change in total precipitable water per daily average rainrate. ERA-40 variables are binned using ERA-40 rainrates (instead of TRMM rainrates) to insure the reliability of the moisture budget components in this case.

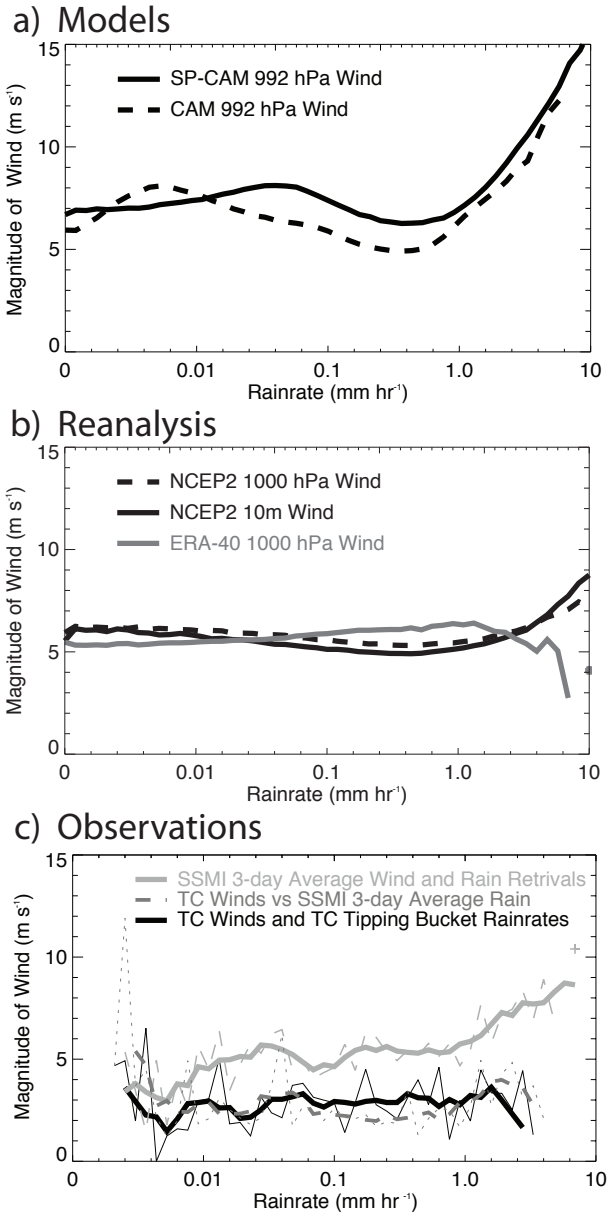

FIG. 7. Composite profiles of daily average lowest level wind magnitude per daily average rainrate. The 998 hPa wind magnitudes are used in panel a, and the 1000 hPa wind magnitudes are used from ERA-40 in panel b. In part c, SSMI 3-day average near-surface wind and rainrate retrievals are also shown for comparison with the TOGA-COARE retrievals. The actual binned values for the observational data are shown as light weight lines, and a five bin running mean is plotted over each as a thicker line.

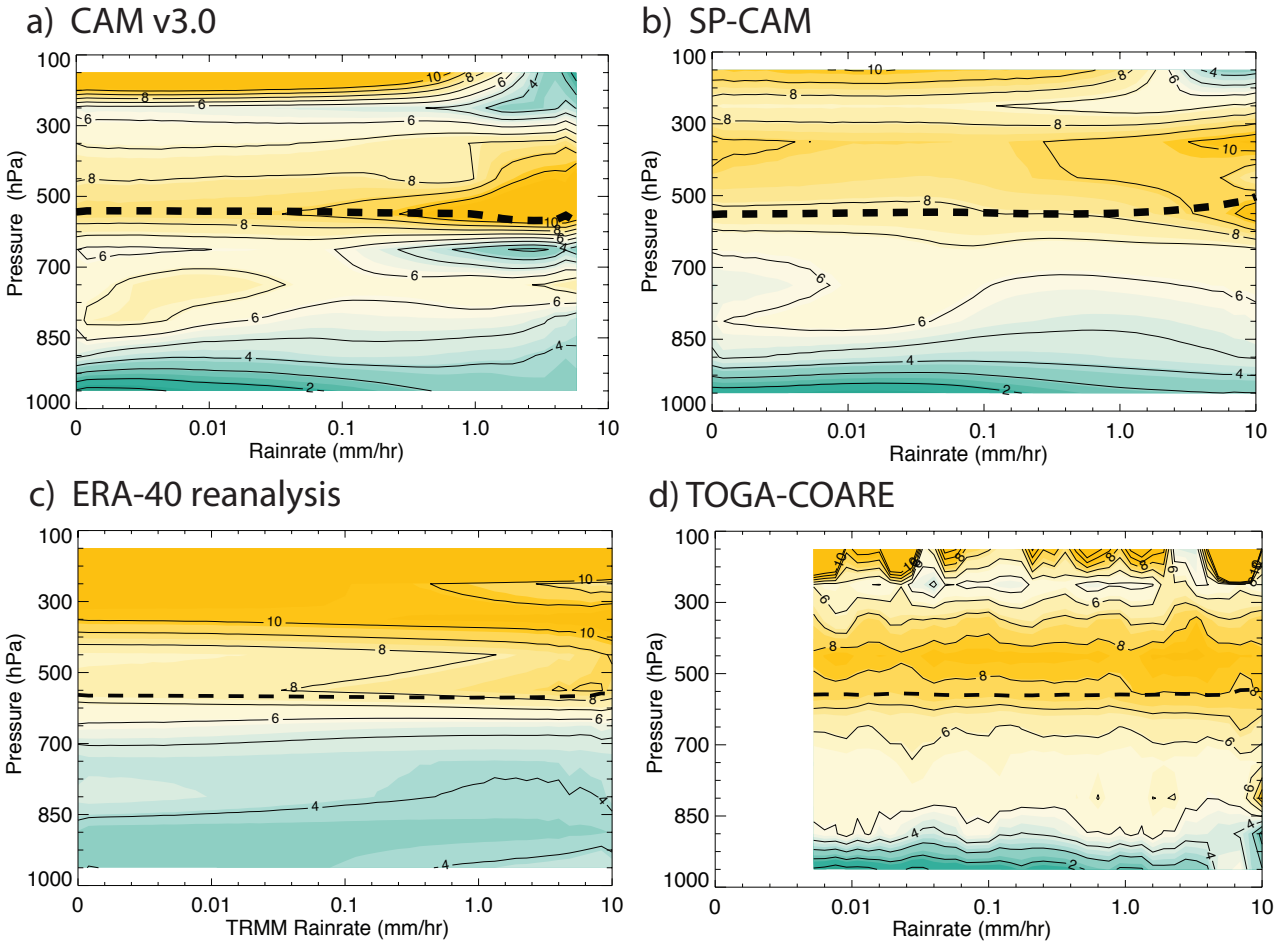

FIG. 8. Composite profiles of daily average static stability (change in potential temperature divided by change in pressure) per value of daily average rainrate. Contour lines are in 10^{-4} K Pa^{-1} increments. The heavy dashed line in each plot is the composite melting level (273.15 K) per rainrate.

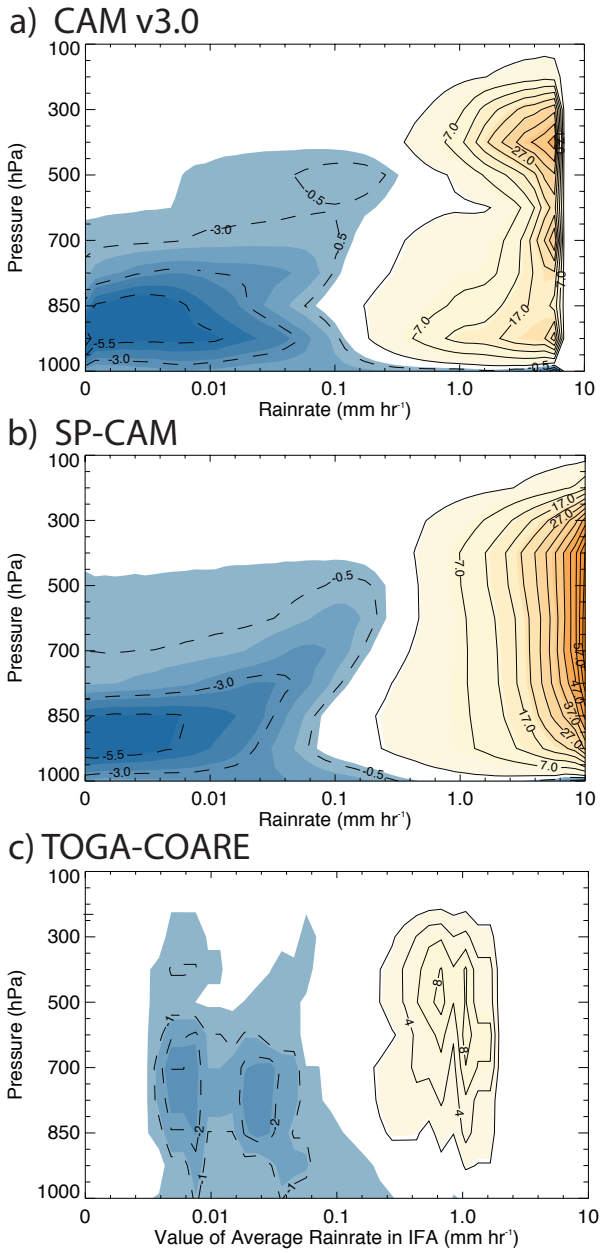

FIG. 9. Composite profiles of daily average Q_2 per value of daily average rainrate. Contour lines are in 2.5 K day^{-1} increments. Negative values (moistening) are dashed contours, and positive values (drying) are solid contours.

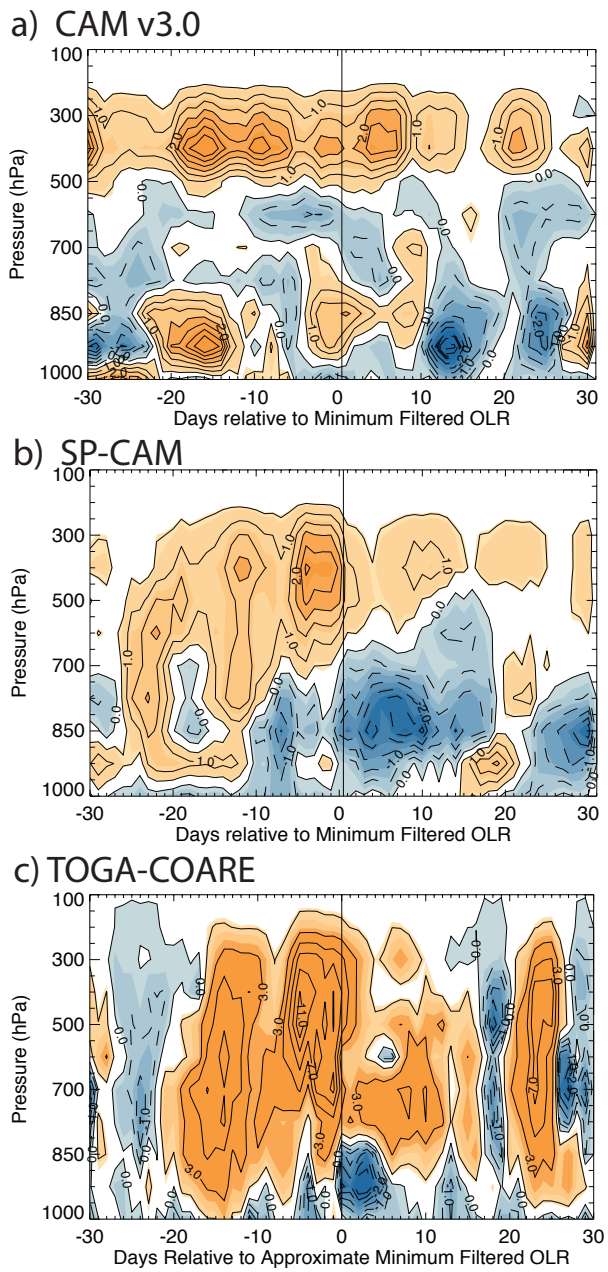

FIG. 10. Composite profiles of daily average Q_2 with the passage of an MJO or large convective event. Contour lines are in 0.5 K day^{-1} increments. Negative values (moistening) are dashed contours, and positive values (drying) are solid contours.

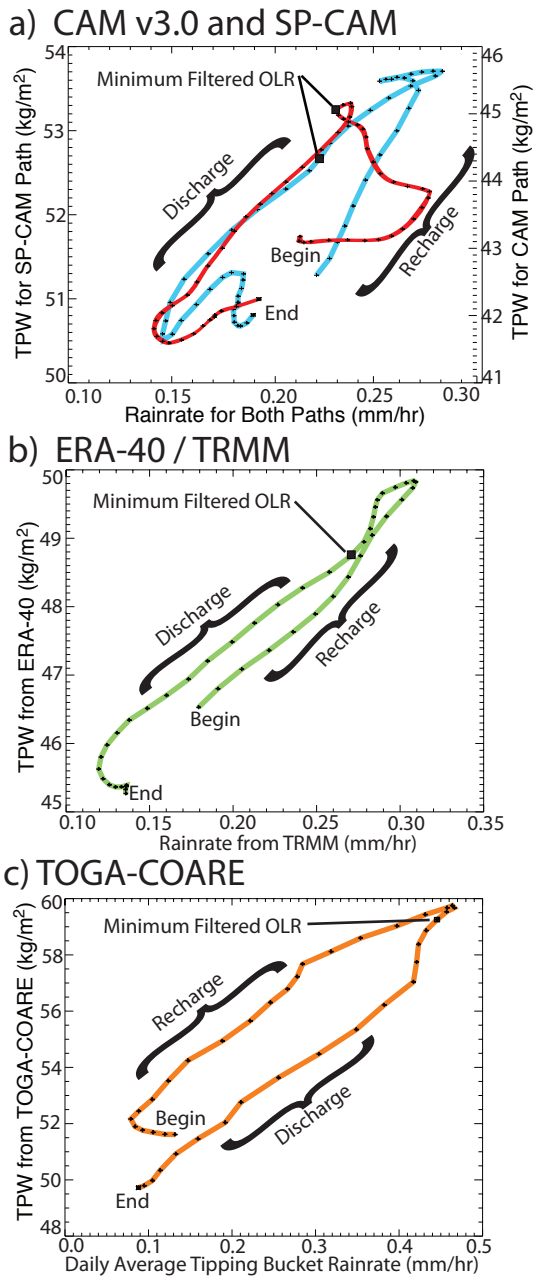

FIG. 11. Plots of rainfall as a function of total precipitable water (TPW) from each day during a composite MJO or strong event. Each point on the line represents the values of rainrate and TPW on a day during the timeline of an event. In panel (a), the red line is the CAM and the blue line the SP-CAM.

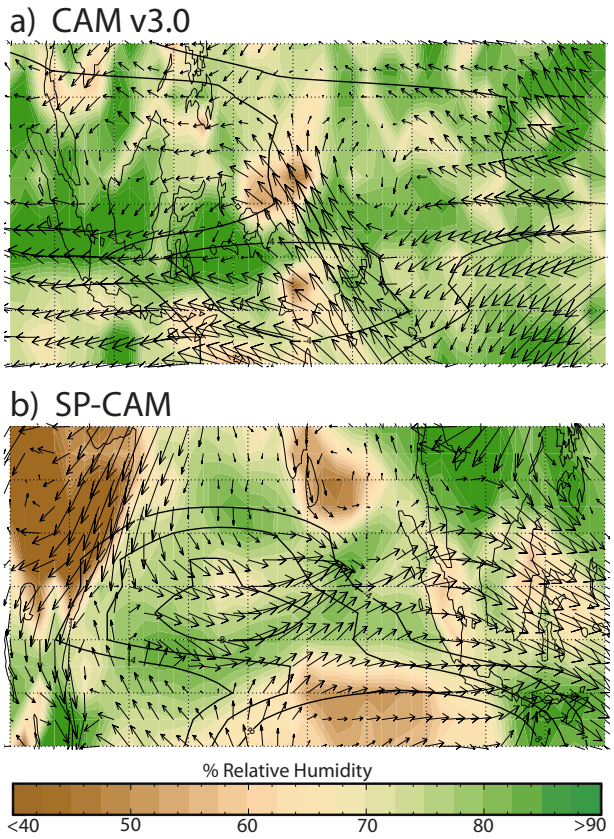

Fig. 12. Maps of the 850 hPa level wind field (arrows) and relative humidity (color contours) and low filtered OLR anomalies (contour lines) on the day of minimum filtered olr for (a) a strong convective event case in the CAM and (b) an MJO case in the SP-CAM. Maximum wind vector magnitudes are (a) 17 m s^{-1} and (b) 19 m s^{-1}.